

Power-law scaling of low-temperature effective mass in La_3ScBi_5

Yi-Ran Li(李祎冉), Yong-Hao Gao(高永豪), Xiao-Qin Lu(卢小琴), Ping Su(苏平), Hui Liang(梁慧), Ying Zhou(周颖), Dan-Dan Wu(吴丹丹), Yan Sun(孙燕), Qiu-Ju Li(李秋菊), Jin-Yu Liu(刘金雨), Shou-Guo Wang(王守国), Gang Chen(陈钢), Tian-Long Xia(夏天龙), Na Li(李娜), Xue-Feng Sun(孙学峰), and Yi-Yan Wang(王义炎)
Citation: Chin. Phys. B, 2026, 35 (**5**): 057107. DOI: 10.1088/1674-1056/ae39d1
http://cpb.iphy.ac.cn; http://iopscience.iop.org/cpb

What follows is a list of articles you may be interested in

Electronic structure of a narrow-gap semiconductor KAg_3Te_2

Rong Feng(冯荣), Haotian Zheng(郑昊天), Haoran Liu(刘浩然), Binru Zhao(赵彬茹), Xunqing Yin(尹训庆), Zhihua Liu(刘智华), Feng Liu(刘峰), Guohua Wang(王国华), Xiaofeng Xu(许晓峰), Wentao Zhang(张文涛), Weidong Luo(罗卫东), Wei Zhou(周苇), and Dong Qian(钱冬)
Chin. Phys. B, 2025, 34 (**4**): 047102. DOI: 10.1088/1674-1056/adb680

The de Haas-van Alphen quantum oscillations in the kagome metal $RbTi_3Bi_5$

Zixian Dong(董自仙), Lei Shi(石磊), Bin Wang(王彬), Mengwu Huo(霍梦五), Xing Huang(黄星), Chaoxin Huang(黄潮欣), Peiyue Ma(马培跃), Yunwei Zhang(张云蔚), Bing Shen(沈冰), and Meng Wang(王猛)
Chin. Phys. B, 2024, 33 (**10**): 107102. DOI: 10.1088/1674-1056/ad6a0a

Prediction of high-mobility two-dimensional electron gas at $KTaO_3$-based heterointerfaces

Fu-Ning Wang(王芙凝), Ji-Chao Li(李吉超), Yi Li(李宜), Xin-Miao Zhang(张鑫淼), Xue-Jin Wang(王学晋), Yu-Fei Chen(陈宇飞), Jian Liu(刘剑), Chun-Lei Wang(王春雷), Ming-Lei Zhao(赵明磊), Liang-Mo Mei(梅良模)
Chin. Phys. B, 2019, 28 (**4**): 047101. DOI: 10.1088/1674-1056/28/4/047101

Density functional theory analysis of electronic structure and optical properties of La-doped Cd_2SnO_4 transparent conducting oxide

Mei Tang(汤梅), Jia-Xiang Shang(尚家香), Yue Zhang(张跃)
Chin. Phys. B, 2018, 27 (**1**): 017101. DOI: 10.1088/1674-1056/27/1/017101

Uniaxial strain-modulated electronic structures of Cd*X* (*X*=S, Se, Te) from first-principles calculations: A comparison between bulk and nanowires

Linlin Xiang(相琳琳), Shenyuan Yang(杨身园)
Chin. Phys. B, 2017, 26 (**8**): 087103. DOI: 10.1088/1674-1056/26/8/087103

RAPID COMMUNICATION

Power-law scaling of low-temperature effective mass in La_3ScBi_5

Yi-Ran Li(李祎冉)[1,†], Yong-Hao Gao(高永豪)[2,†], Xiao-Qin Lu(卢小琴)[3,†], Ping Su(苏平)[1], Hui Liang(梁慧)[1], Ying Zhou(周颖)[1], Dan-Dan Wu(吴丹丹)[1], Yan Sun(孙燕)[1], Qiu-Ju Li(李秋菊)[4], Jin-Yu Liu(刘金雨)[5], Shou-Guo Wang(王守国)[1], Gang Chen(陈钢)[6,7], Tian-Long Xia(夏天龙)[8,9,10,‡], Na Li(李娜)[1,§], Xue-Feng Sun(孙学峰)[1,¶], and Yi-Yan Wang(王义炎)[1,#]

[1] *Anhui Provincial Key Laboratory of Magnetic Functional Materials and Devices, Institutes of Physical Science and Information Technology, Anhui University, Hefei* 230601, *China*
[2] *Tsung-Dao Lee Institute, Shanghai Jiao Tong University, Shanghai* 201210, *China*
[3] *School of Physics and Information Engineering, Guangdong University of Education, Guangzhou* 510303, *China*
[4] *School of Physics and Optoelectronic Engineering, Anhui University, Hefei* 230601, *China*
[5] *Department of Physics and Astronomy, University of California, Irvine, CA*, 92617, *USA*
[6] *International Center for Quantum Materials, School of Physics, Peking University, Beijing* 100871, *China*
[7] *Collaborative Innovation Center of Quantum Matter, Beijing* 100871, *China*
[8] *School of Physics and Beijing Key Laboratory of Opto-electronic Functional Materials & Micro-nano Devices, Renmin University of China, Beijing* 100872, *China*
[9] *Key Laboratory of Quantum State Construction and Manipulation (Ministry of Education), Renmin University of China, Beijing* 100872, *China*
[10] *Laboratory for Neutron Scattering, Renmin University of China, Beijing* 100872, *China*

(Received 10 November 2025; revised manuscript received 17 January 2026; accepted manuscript online 19 January 2026)

The variation of the effective mass m^* of carrier is often overlooked in experimental studies on quantum oscillations and Kohler's rule. Here, we report the magnetotransport properties of La_3ScBi_5 and reveal the changing m^* in it. The temperature and magnetic field dependence of m^* follows the power-law scaling behavior at low temperature and leads to the failure of conventional analysis, which should not be ignored. In the analysis of the thermal factor and Dingle plot of de Haas–van Alphen oscillation in La_3ScBi_5, satisfactory fitting results can be obtained after considering the correction of m^*. We have also applied this method to $Sr_{1-y}Mn_{1-z}Sb_2$, solving the remaining fitting problem in previous reports. Moreover, the magnetoresistance (MR) of La_3ScBi_5 has been found to violate Kohler's rule. Although the extended Kohler's rule is applicable to high-temperature MR data, it does not scale the low-temperature data well. We further modified the extended Kohler's rule by introducing m^*, and subsequently scaled the low-temperature MR data well. Our study emphasizes the importance of considering the variation of m^* in the analysis of quantum oscillations and Kohler's rule, and provides a method for extracting the temperature and magnetic field dependence of m^* through quantum oscillations, which is very beneficial for the data analysis of other materials in the future.

Keywords: effective mass, quantum oscillations, Kohler's rule, topological material

PACS: 71.38.Cn, 75.47.–m, 73.43.Qt, 74.25.F–

DOI: 10.1088/1674-1056/ae39d1 **CSTR:** 32038.14.CPB.ae39d1

1. Introduction

Quantum oscillation has been a powerful experimental technique for exploring the underlying physics in materials. Quantum oscillations mainly include the de Haas–van Alphen (dHvA) oscillation in magnetization and the Shubnikov–de Haas oscillation in resistivity. Recently, Wang *et al.* discovered a new type of quantum oscillation with the log$B$ periodicity in $ZrTe_5$.[1] Chen *et al.* observed the oscillation of resistivity and specific heat with temperature under a constant magnetic field in NdAlSi.[2] The Lifshitz–Kosevich (LK) theory is commonly used to describe the quantum oscillations.[3] By analyzing the quantum oscillations using the LK formula, some parameters can be obtained, such as the effective mass m^*, Dingle temperature, and Berry phase.

Kohler's rule is an important law related to the magnetoresistance (MR) of materials, which states that the MR should be a function of B/ρ_0 and follow the scaling behavior $\mathrm{MR} = f(B/\rho_0)$ (ρ_0 is the resistivity at zero field).[4] Luo *et al.* pointed out that the more exact form of Kohler's rule is $\mathrm{MR} = f(B\tau)$ with τ being the relaxation time of carriers.[5] Recently, Xu *et al.* proposed the extended Kohler's rule $\mathrm{MR} = f(B/n_{\mathrm{T}}\rho_0)$, where n_{T} describes the relative change in

†These authors contributed equally to this work.
‡Corresponding author. E-mail: tlxia@ruc.edu.cn
§Corresponding author. E-mail: nli@ahu.edu.cn
¶Corresponding author. E-mail: xfsun@ahu.edu.cn
#Corresponding author. E-mail: wyy@ahu.edu.cn

© 2026 Chinese Physical Society and IOP Publishing Ltd. All rights, including for text and data mining, AI training, and similar technologies, are reserved.

the carrier concentration induced by thermal excitation.[6] The extended Kohler's rule can effectively explain the violation of Kohler's rule in some materials,[6–8] such as TaP, InSb, $TaCo_2Te_2$, and $HfSe_{1.9}$.

However, whether in the analysis of quantum oscillations or Kohler's rule, m^* is always treated as an invariant constant. In this paper, we have studied the dHvA oscillations and Kohler's rule in La_3ScBi_5 and found that the temperature and magnetic field dependence of m^* should not be ignored. m^* follows the power-law scaling behavior at low temperature due to the effective mass renormalization by the long-range Coulomb interaction. The conventional analysis based on the LK formula fails to fit the oscillation data of La_3ScBi_5. The better fits are obtained after considering the correction of m^*, indicating that m^* in La_3ScBi_5 changes with temperature and magnetic field. In addition, the MR has been found to violate Kohler's rule, and even the use of extended Kohler's rule is not enough for scaling the low-temperature data. By introducing the magnetic field and temperature dependence of m^* obtained from the quantum oscillation, the extended Kohler's rule is further modified to $\mathrm{MR} = f(Bm^*/n_T\rho_0)$, which can effectively scale the low-temperature MR data.

2. Results and discussion

La_3ScBi_5 is a member of the Ln_3MPn_5 (Ln = lanthanide; M = metal; Pn = pnictide) family,[9–17] and its crystal structure contains 1D Bi chain and a distorted kagome lattice.[18] The band structure calculations reveal that multiple types of Dirac fermions coexist in La_3ScBi_5, including type-I, type-II, higher-order quadratic and nodal-line.[18]

Figures 1(a)–1(c) plot the isothermal magnetization of La_3ScBi_5 as a function of magnetic field in the directions of $B \perp bc$, $B \parallel b$ and $B \parallel c$, respectively. Strong dHvA quantum oscillations can be observed in these three directions under low temperature and strong magnetic field. For the directions within the distorted kagome lattice plane ($B \perp bc$ and $B \parallel b$), there are small kinks induced by the Zeeman effect in high fields [red arrows in Figs. 1(a) and 1(b)], similar to those in ZrGeSe[19] and Sn_4P_3.[20] In low fields, it seems to have a very low-frequency oscillation. This possible low-frequency oscillation has little impact on high magnetic field amplitude, but it will affect the background extraction of high-frequency oscillations. For the accuracy of the analysis of high field oscillation, such a low-frequency oscillation is ignored when extracting the background. The insets of Figs. 1(d)–1(f) show the oscillatory components of magnetization ($\Delta M = M - \langle M \rangle$) after subtracting the smooth background $\langle M \rangle$. The corresponding fast Fourier transformation (FFT) spectra are displayed in the main images of Figs. 1(d)–1(f).

The anisotropy of magnetization in La_3ScBi_5 is interesting. The magnetization is dominated by paramagnetism in the $B \perp bc$ and $B \parallel b$ directions, but exhibits diamagnetism in the long-axis direction ($B \parallel c$). This situation is different from the unusual axial diamagnetism in La_3MgBi_5, where the magnetization is dominated by diamagnetism in the directions of the crystal axis ($B \parallel a, b, c$).[11] The axial diamagnetism in La_3MgBi_5 originates from the restricted motion of the Dirac fermion at the Fermi level. The anisotropic magnetization in La_3ScBi_5 can be attributed to the type-I Dirac fermion located near the Fermi level in the Γ–A direction.

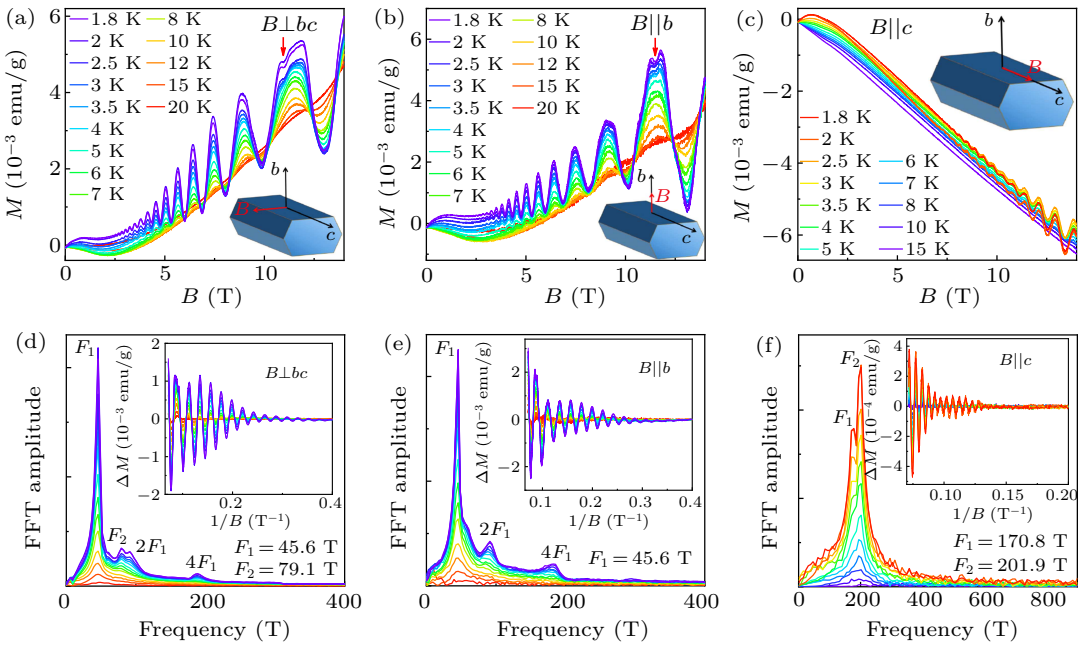


Fig. 1. The dHvA oscillations in La_3ScBi_5. (a)–(c) Magnetic field dependence of magnetization in three directions at various temperatures. The magnetic field follows the directions of $B \perp bc$, $B \parallel b$ and $B \parallel c$, respectively. The measurements were performed on the same sample and the same quartz rod. Insets: The schematic diagrams of the measurements. (d)–(f) The FFT spectra of the oscillations. Insets: The oscillation amplitude ΔM as a function of $1/B$.

The dHvA quantum oscillation can be described by the LK formula[3,21–23]

$$\Delta M \propto -B^{1/2} R_{\rm T} R_{\rm D} \sin\left[2\pi\left(\frac{F}{B}-\frac{1}{2}+\beta+\delta\right)\right]; \quad (1)$$

$$R_{\rm T} = \frac{\lambda T}{\sinh(\lambda T)}; \quad R_{\rm D} = {\rm e}^{-\lambda T_{\rm D}}; \quad (2)$$

$$\lambda = (2\pi^2 k_{\rm B} m^*)/(\hbar e B). \quad (3)$$

In the formula, $R_{\rm T}$ and $R_{\rm D}$ represent the variation of oscillation amplitude with temperature and magnetic field, respectively. m^* is the cyclotron effective mass of carrier. $T_{\rm D}$ is the Dingle temperature. $2\pi\beta$ is the Berry phase and δ is a phase shift. The thermal factor $R_{\rm T}$ is often used to fit the temperature dependence of FFT amplitude and extract the effective mass m^*. The main image in Fig. 2(a) shows the $R_{\rm T}$ fittings of frequency F_1 in the $B \perp bc$ direction. The black solid line is the fit made by including all obtained data points. Clearly, conventional thermal factor $R_{\rm T}$ cannot describe the data well. A better fit can be obtained if the data points below 5 K are not included [red solid line in Fig. 2(a)]. Here, we propose that the failure of conventional $R_{\rm T}$ fitting can be attributed to changes in the effective mass m^* of carrier. In previous studies on quantum oscillations, m^* was always treated as a constant. However, in reality, m^* can vary with temperature.[6,24] By considering the influence of the long-range Coulomb interaction,[18,25] the dependence of m^* on temperature can be taken as $m^* \propto (T+T_0)^{m_1}$, and then the temperature term in $R_{\rm T}$ becomes $T(T+T_0)^{m_1}$ ($m_1 = 0$ corresponds to the conventional $R_{\rm T}$). As shown in Fig. 2(d), the data can be well fitted using this modified $R_{\rm T}$, and the goodness-of-fit has increased from 0.9807 (F_1) / 0.9743 (F_2) to 0.9951 (F_1) / 0.9949 (F_2). For frequencies F_1 and F_2 in the $B \perp bc$ direction, the m^* terms obtained by fitting are $(T+0.60)^{-0.36}$ and $(T+1.83)^{-0.45}$, respectively. The frequency in the $B \parallel b$ direction exhibits a similar phenomenon [Figs. 2(b) and 2(e)]. The modified $R_{\rm T}$ fitting improved the goodness-of-fit from 0.9916 to 0.9997 and generated a m^* term $(T+2.83)^{-0.37}$. The situation is different in the $B \parallel c$ direction, and using conventional $R_{\rm T}$ to fit can produce acceptable results [Fig. 2(c)], which means that the temperature dependence of m^* in this direction is relatively weak. However, it should be noted that using the modified $R_{\rm T}$ can achieve better fittings [Fig. 2(f)]. The obtained m^* terms for frequencies F_1 and F_2 in the $B \parallel c$ direction are $(T+1.97)^{-0.20}$ and $(T+2.87)^{-0.20}$, respectively.

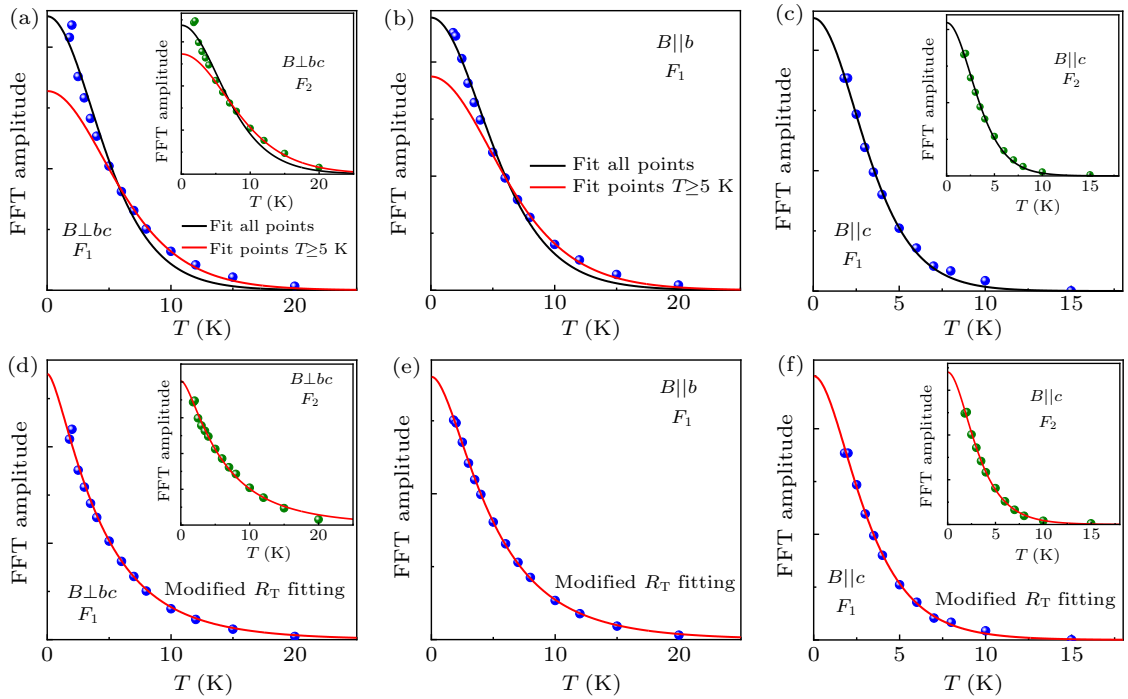


Fig. 2. (a), (d) $R_{\rm T}$ fittings and modified $R_{\rm T}$ fitting of oscillation frequency F_1 in the $B \perp bc$ direction. The insets show the corresponding fittings of the frequency F_2. (b), (e) $R_{\rm T}$ fittings and modified $R_{\rm T}$ fitting of the frequency F_1 in the $B \parallel b$ direction. In (a) and (b), the black and red solid lines represent the $R_{\rm T}$ fittings for all points and points with $T \geq 5$ K, respectively. (c), (f) $R_{\rm T}$ fitting and modified $R_{\rm T}$ fitting of the frequency F_1 in the $B \parallel c$ direction. The insets show the corresponding fittings of the frequency F_2.

By comparing the fitting results of the three directions in Fig. 2, three main conclusions can be drawn. (i) The temperature dependence of m^* has a significant impact on the amplitude of quantum oscillations. The stronger the temperature dependence of m^* (m_1 deviates from 0), the worse the description of oscillation amplitude by conventional $R_{\rm T}$. (ii) The modified $R_{\rm T}$ can fit the data well and extract the temperature dependent behavior of m^*. (iii) The temperature dependence of m^* in La_3ScBi_5 exhibits obvious anisotropy, which is stronger in the distorted kagome lattice plane but weaker in the long-axis direction. In La_3ScBi_5, the effective mass follows the power-law scaling behavior $m^* \propto (T+T_0)^{m_1}$ at low temper-

ature. In fact, such a temperature dependent behavior of m^* has been theoretically obtained in three-dimensional systems with long-range Coulomb interaction.[25] The numerical calculation results show that the temperature dependence of m^* is only significant under long-range Coulomb interaction, indicating a close relationship between them.[25] Similar power-law scaling behavior of m^* also appears in some strongly correlated systems, such as heavy fermions,[26] which is not the case in La_3ScBi_5. The electron–phonon interaction is also not expected to dominate the correction of m^*, as m^* follows the power-law scaling behavior and increases with decreasing temperature, but the phonon occupation number decreases at low temperatures. The above results not only indicate the validity of the modified R_T, but also suggest that the long-range Coulomb interaction plays an important role in La_3ScBi_5 and causes the changes of m^*. Especially, this method is universal and can also be applied to other materials, such as an established magnetic topological semimetal $Sr_{1-y}Mn_{1-z}Sb_2$.[18,22]

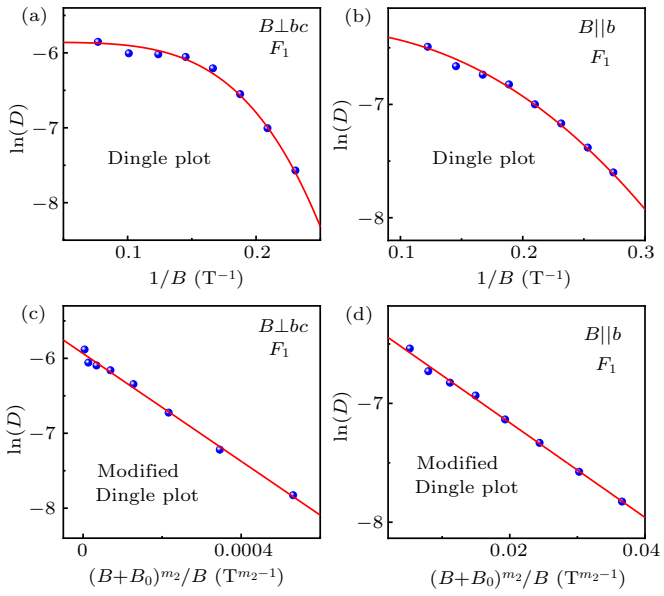


Fig. 3. (a), (b) The Dingle plots of F_1 in the $B \perp bc$ and $B \parallel b$ directions. The red solid lines are the fits by considering $m^* \propto (B+B_0)^{m_2}$. The data points were extracted from the valleys of ΔM at 1.8 K in the insets of Figs. 2(d) and 2(e). For the $B \parallel b$ direction, the two valleys under high field are excluded in (b) due to the large influence of harmonic frequency. (c), (d) The modified Dingle plots of F_1 in the $B \perp bc$ and $B \parallel b$ directions. The values of m_2 and B_0 obtained from (a) and (b) were used to correct the power exponent of B on the horizontal and vertical axes.

Since m^* can vary with temperature, it is natural to wonder if m^* will vary with a magnetic field. This question can be explored by studying the Dingle plot. According to the LK formula, if $\ln[D]$ $[D = \Delta M\sqrt{B}\sinh(\lambda T)]$ is plotted as a function of $1/B$, the image will be a linear line with a fixed slope. Such a Dingle plot is often used to extract Dingle temperature T_D from the fitted slope. However, the premise of the above operation is that m^* does not change with B. Figures 3(a) and 3(b) show the conventional Dingle plots of F_1 in the $B \perp bc$ and $B \parallel b$ directions, respectively. Clearly, the data points do not present a straight line, indicating a nonlinear relationship between $\ln[D]$ and $1/B$. Similar to the temperature dependence of m^*, taking $m^* \propto (B+B_0)^{m_2}$, the magnetic field term in R_D will become $(B+B_0)^{m_2}/B$ ($m_2 = 0$ corresponds to the conventional R_D). As shown by the red solid lines in Figs. 3(a) and 3(b), the data can be well fitted after considering the magnetic field dependence of m^*. The obtained m^* terms are $(B+0.63)^{-3.79}$ and $(B+0.25)^{-1.48}$, respectively. Furthermore, the Dingle plot can be modified using fitted values of m_2 and B_0. If the power exponent of B in the horizontal and vertical axes is corrected to $(B+B_0)^{m_2}/B$, the data points will fall on a straight line [Figs. 3(c) and 3(d)], which returns to the linear description of the conventional Dingle plot. Therefore, in La_3ScBi_5, the magnetic field will have a significant impact on m^*. The magnetic field dependent m^* may be another characteristic of long-range Coulomb interaction systems, which requires further theoretical research.

After characterizing the magnetic properties, the electrical transport properties of La_3ScBi_5 have also been investigated. As shown in the inset of Fig. 4(a), the resistivity of La_3ScBi_5 exhibits the metallization behavior. Figures 4(a) and 4(b) show the MR in the range of 1.8 K–25 K and 30 K–300 K, respectively. The curvature of the MR curves varies at different temperatures. The curves are concave at temperatures above 30 K. However, the curves become convex at temperatures below 25 K, which is the result of the weak antilocalization effect.[27,28] The MR data for the entire temperature range can be well fitted using the typical power law MR $\propto B^t$. The obtained values of t are presented in the inset of Fig. 4(b). The variation of t can also clearly reflect the concavity and convexity of the curves.

Figure 4(c) shows the MR of La_3ScBi_5 plotted against B/ρ_0. Clearly, the MR curves at different temperatures do not collapse onto a single curve, indicating the violation of Kohler's rule MR $= f(B/\rho_0)$. The violation of Kohler's rule in La_3ScBi_5 is not expected, as the Hall resistivity exhibits a single band behavior.[18] In order to further understand the MR behavior, the extended Kohler's rule MR $= f(B/n_T\rho_0)$ has been employed to scale the MR data. As shown in Fig. 4(d), the curves can roughly collapse onto a single curve. Although the extended Kohler's rule can effectively scale the MR data above 30 K, it is not ideal for data below 30 K. There are two interesting phenomena that need to be noted here. Firstly, the carrier concentration of La_3ScBi_5 is high.[18] The violation of Kohler's rule is more commonly observed in topological semimetals or semiconductors, as their low carrier concentration makes the thermal factor n_T more sensitive to temperature.[6] For typical metals with high carrier concentration, n_T becomes less sensitive to the change of temperature. However, La_3ScBi_5 has a high carrier concentration and exhibits a clear violation of Kohler's rule. This may indicate that

the Dirac fermions near the Fermi level dominate electrical transport in La_3ScBi_5. Secondly, the curves in Fig. 4(d) only roughly collapse onto one curve but do not completely overlap, which means that even the extended Kohler's rule cannot perfectly describe the case in La_3ScBi_5.

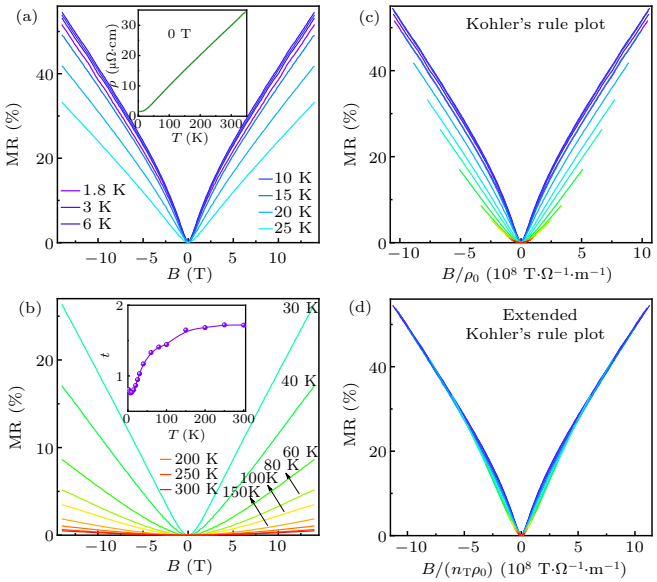


Fig. 4. (a) Magnetic field dependent MR of La_3ScBi_5 in the range of 1.8 K to 25 K. Inset: Temperature dependent resistivity of La_3ScBi_5 at zero field. (b) Magnetic field dependent MR of La_3ScBi_5 in the range of 30 K to 300 K. Inset: The power exponent n extracted from the fits using MR $\propto B^t$. (c) Kohler's rule plot of the MR curves. (d) Extended Kohler's rule plot of the MR curves.

In fact, a modified scaling form MR $= f(B\tau)$ has been introduced in a previous study,[5] where τ is the relaxation time of carriers. $B\tau$ can be represented as $B\tau = (m^*/e^2)B/(n\rho_0)$ by using $\rho_0 = m^*/(ne^2\tau)$. Therefore, the scaling behavior MR $= f(B/n_T\rho_0)$ of the extended Kohler's rule will be obtained if m^* is temperature independent.[6] Even if m^* is not temperature independent, the extended Kohler's rule is still valid because the influence of temperature on m^* can be included in n_T. However, the magnetic field dependence of m^* has been ignored in the above analysis. By introducing the temperature and magnetic field dependence of m^*, the extended Kohler's rule can be further modified to MR $= f(Bm^*/n_T\rho_0)$. As shown in Fig. 5, after considering the variation of m^*, the MR curves at low temperature are well scaled onto a single curve, indicating that the failure of the extended Kohler's rule at low temperature comes from the change of m^* with magnetic field. The introduction of m^* will lead to the change of curve behavior. Unlike the Kohler's rule or the extended Kohler's rule, here the x-axis variable has changed from B to $B(B+B_0)^{m_2}$. In the current analysis of La_3ScBi_5, as the magnetic field increases, the value of $B(B+B_0)^{m_2}$ will first increase and then decrease, resulting in the curve behavior shown in Fig. 5. However, no matter how the curve behavior changes, the MR curves at low temperature can still be well scaled to the same curve, indicating the effectiveness of the modification of the extended Kohler's rule by m^*.

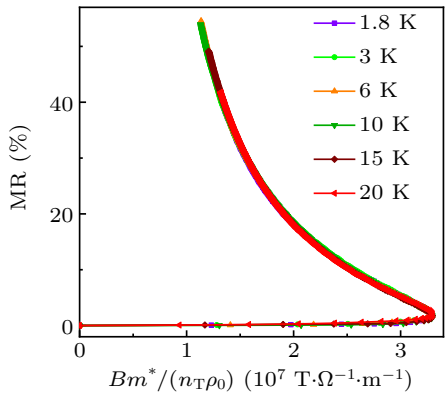


Fig. 5. Further modification to the extended Kohler's rule. The MR scaling in the temperature range of 1.8–20 K, in which the magnetic field and temperature dependence of m^* are introduced instead of treating it as a constant.

3. Summary

In summary, we have grown high-quality single crystals of La_3ScBi_5, which exhibit strong dHvA quantum oscillations. In the process of analyzing quantum oscillations, it was found that m^* changes with temperature and magnetic field rather than remaining a constant, leading to the failure of conventional fits. The better fits have been obtained through the correction of m^*. The MR of La_3ScBi_5 exhibits a violation of Kohler's rule. Even the extended Kohler's rule is only applicable to scaling the high-temperature data. The extended Kohler's rule is further modified by considering the variability of m^*, after which the MR at low temperature can be well scaled.

Acknowledgements

This work is supported by the National Key R&D Program of China (Grant Nos. 2023YFA1406500, 2024YFA1409002, and 2021YFA1400300), the National Natural Science Foundation of China (Grant Nos. 12474098, 12574042, 12274388, 12404043, 12074425, and 12204004), the Natural Science Foundation of Anhui Province (Grant No. 2408085QA024), the Science and Technology Projects in Guangzhou (Grant No. 2023A04J1936), the Fundamental Research Funds for the Central Universities (Peking University), the Research Funds of Renmin University of China (Grant No. 23XNKJ22), and the Beijing National Laboratory for Condensed Matter Physics (Grant No. 2023BNLCMPKF008).

References

[1] Wang H, Liu H, Li Y, Liu Y, Wang J, Liu J, Dai J Y, Wang Y, Li L, Yan J, Mandrus D, Xie X C and Wang J 2018 *Sci. Adv.* **4** eaau5096
[2] Wang J F, Dong Q X, Huang Y F, Wang Z S, Guo Z P, Wang Z J, Ren Z A, Li G, Sun P J, Dai X and Chen G F 2023 *Phys. Rev. B* **108** 024423
[3] Shoenberg D 1984 *Magnetic oscillations in metals* (Cambridge: Cambridge University Press)
[4] Kohler M 1938 *Ann. Phys.* **424** 211
[5] Luo N and Miley G 2002 *Physica C* **371** 259

[6] Xu J, Han F, Wang T T, Thoutam L R, Pate S E, Li M, Zhang X, Wang Y L, Fotovat R, Welp U, Zhou X, Kwok W K, Chung D Y, Kanatzidis M G and Xiao Z L 2021 *Phys. Rev. X* **11** 041029

[7] Pate S, Chen B, Shen B, Li K, Zhou X, Chung D Y, Divan R, Kanatzidis M G, Welp U, Kwok W K and Xiao Z L 2024 *Phys. Rev. B* **109** 035129

[8] Liu W, Zheng Y, Kondusamy A L N, Scherm D L, Malko A V and Lv B 2024 *Phys. Rev. Mater.* **8** 054006

[9] Khoury J F, Han B, Jovanovic M, Singha R, Song X, Queiroz R, Ong N P and Schoop L M 2022 *J. Am. Chem. Soc.* **144** 9785

[10] Han X, Pi H, Yan D, Zhang R, Li Y, Wang X, Dun Z, Wang Z, Feng H L, Wu Q and Shi Y 2023 *Phys. Rev. B* **108** 075157

[11] Yi Z K, Ouyang Z F, Guo P J, Liang H, Li Y R, Su P, Li N, Zhou Y, Wu D D, Sun Y, Yue X Y, Li Q J, Wang S G, Sun X F and Wang Y Y 2024 *Adv. Mater.* **36** 2400166

[12] Han X, Li Y, Yang M, Miao S, Yan D and Shi Y 2023 *Phys. Rev. Mater.* **7** 124406

[13] Khoury J F, Han B, Jovanovic M, Queiroz R, Yang X, Singha R, Salters T H, Pollak C J, Lee S B, Ong N and Schoop L M 2024 *Adv. Mater.* **36** 2404553

[14] Zhang C, Wang Y, Zheng J, Du L, Li Y, Han X, Liu E, Wu Q and Shi Y 2024 *Phys. Rev. Mater.* **8** 034402

[15] Duan L, Wang X C, Zhang J, Hu Z, Zhao J F, Feng Y G, Zhang H L, Lin H J, Chen C T, Wu W, Li Z, Wang R, Zhang J F, Xiang T and Jin C Q 2022 *Phys. Rev. B* **106** 184405

[16] Duan L, Wang X, Zhan F, Zhang J, Hu Z, Zhao J, Li W, Cao L, Deng Z, Yu R, Lin H J, Chen C T, Wang R and Jin C 2020 *Sci. China-Mater.* **63** 1750

[17] Wang Y Y, Yi Z K, Li N, Li Y R, Su P, Zhou Y, Wu D D, Sun Y, Li Q J, Yue X Y, Zhao X, Sun X F and Liang H 2024 *Phys. Rev. B* **110** 134432

[18] See supplemental material for some additional data, including the experimental methods, crystal structure, electronic structure, angle dependent dHvA oscillation, Hall resistivity, negative longitudinal MR, the application of changing carrier effective mass in $Sr_{1-y}Mn_{1-z}Sb_2$, and the calculated m^* renormalization by the long-range Coulomb interaction.

[19] Hu J, Zhu Y L, Graf D, Tang Z J, Liu J Y and Mao Z Q 2017 *Phys. Rev. B* **95** 205134

[20] Liu Q, Guo P J, Xu S, Yue X Y, Wang H, Wang X Y, Liang H, Wu D D, Sun Y, Li Q J, Xia T L, Sun X F and Wang Y Y 2023 *J. Phys. Chem. C* **127** 4319

[21] Hu J, Tang Z, Liu J, Liu X, Zhu Y, Graf D, Myhro K, Tran S, Lau C N, Wei J and Mao Z 2016 *Phys. Rev. Lett.* **117** 016602

[22] Liu J, Hu J, Zhang Q, Graf D, Cao H, Radmanesh S, Adams D, Zhu Y, Cheng G, Liu X, Phelan W, Wei J, Jaime M, Balakirev F, Tennant D, DiTusa J, Chiorescu I, Spinu L and Mao Z 2017 *Nat. Mater.* **16** 905

[23] Wang Y Y, Xu S, Sun L L and Xia T L 2018 *Phys. Rev. Mater.* **2** 021201

[24] Kimura S i, Yokoyama H, Watanabe H, Sichelschmidt J, Süß V, Schmidt M and Felser C 2017 *Phys. Rev. B* **96** 075119

[25] Zhang Y and Das Sarma S 2004 *Phys. Rev. B* **70** 035104

[26] Shaginyan V, Amusia M Y, Msezane A and Popov K 2010 *Phys. Rep.* **492** 31

[27] OuYang H, Dong Q X, Huang Y F, Xiang J S, Zhang L B, Li C S, Sun P J, Ren Z A and Chen G F 2021 *Chin. Phys. B* **30** 127101

[28] Yi Z K, Liu Q, Guang S K, Xu S, Yue X Y, Liang H, Li N, Zhou Y, Wu D D, Sun Y, Li Q J, Cheng P, Xia T L, Sun X F and Wang Y Y 2024 *Chin. Phys. B* **33** 047501